iScience

CellPress
OPEN ACCESS

Article

Enhanced and copper concentration dependent virucidal effect against SARS-CoV-2 of electrospun poly(vinylidene difluoride) filter materials

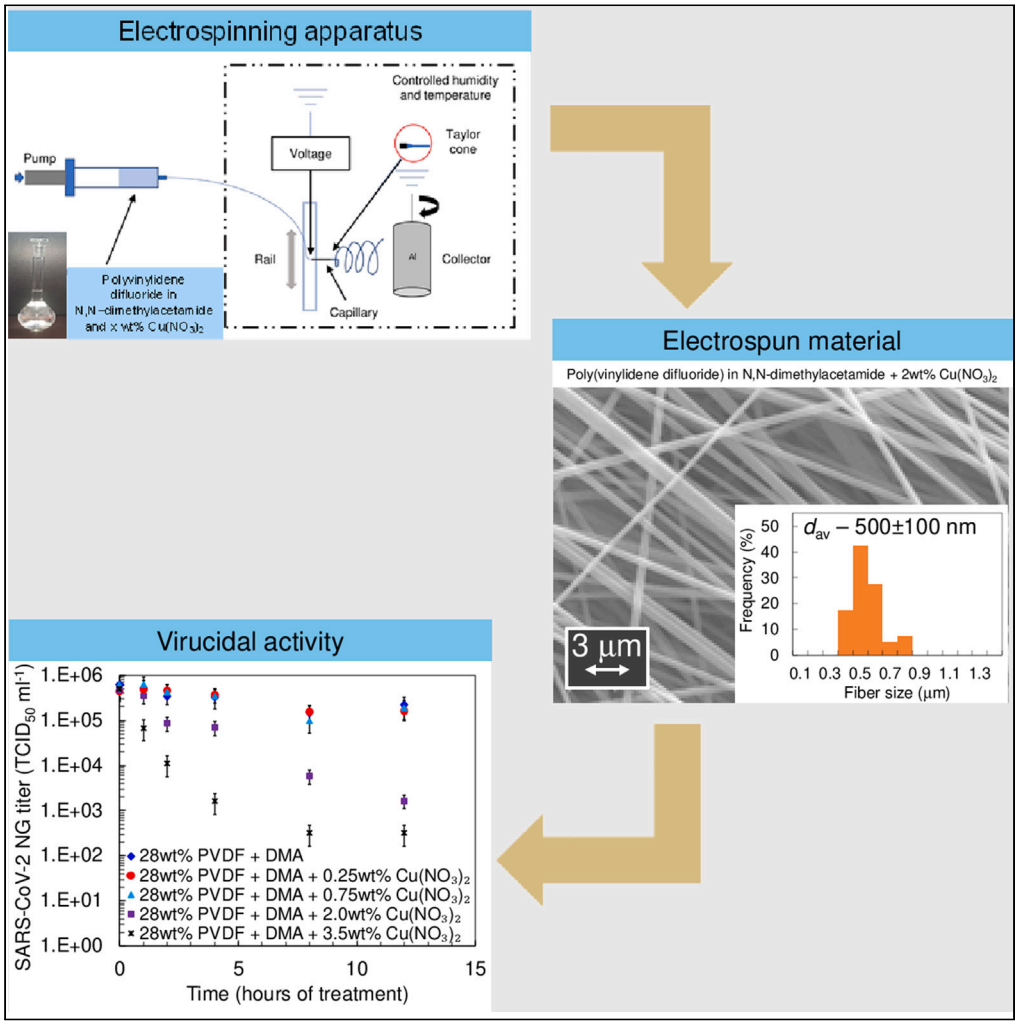

Hanna Bulgarin, Thomas Thomberg, Andres Lust, ..., Liane Viru, Andres Merits, Enn Lust

thomas.thomberg@ut.ee

Highlights

Cu containing fibrous materials were prepared by electrospinning method

$Cu(NO_3)_2 \cdot 2.5H_2O$ transformed into $Cu_2(NO_3)(OH)_3$ during electrospinning process

Cu nanoclusters containing material showed very high filtration efficiency

Cu containing material showed very high virudical activity against SARS-CoV-2

Bulgarin et al., iScience 27, 109835
June 21, 2024
https://doi.org/10.1016/j.isci.2024.109835

iScience

CellPress
OPEN ACCESS

Article

Enhanced and copper concentration dependent virucidal effect against SARS-CoV-2 of electrospun poly(vinylidene difluoride) filter materials

Hanna Bulgarin,[1] Thomas Thomberg,[1,7,*] Andres Lust,[2] Jaak Nerut,[1] Miriam Koppel,[1] Tavo Romann,[1] Rasmus Palm,[1,3] Martin Månsson,[3] Marko Vana,[4] Heikki Junninen,[4] Marian Külaviir,[5] Päärn Paiste,[5] Kalle Kirsimäe,[5] Marite Punapart,[6] Liane Viru,[6] Andres Merits,[6] and Enn Lust[1]

SUMMARY

Virucidal filter materials were prepared by electrospinning a solution of 28 wt % poly(vinylidene difluoride) in N,N-dimethylacetamide without and with the addition of 0.25 wt %, 0.75 wt %, 2.0 wt %, or 3.5 wt % $Cu(NO_3)_2 \cdot 2.5H_2O$ as virucidal agent. The fabricated materials had a uniform and defect free fibrous structure and even distribution of copper nanoclusters. X-ray diffraction analysis showed that during the electrospinning process, $Cu(NO_3)_2 \cdot 2.5H_2O$ changed into $Cu_2(NO_3)(OH)_3$. Electrospun filter materials obtained by electrospinning were essentially macroporous. Smaller pores of copper nanoclusters containing materials resulted in higher particle filtration than those without copper nanoclusters. Electrospun filter material fabricated with the addition of 2.0 wt % and 3.5 wt % of $Cu(NO_3)_2 \cdot 2.5H_2O$ in a spinning solution showed significant virucidal activity, and there was 2.5 ± 0.35 and 3.2 ± 0.30 logarithmic reduction in the concentration of infectious SARS-CoV-2 within 12 h, respectively. The electrospun filter materials were stable as they retained virucidal activity for three months.

INTRODUCTION

The SARS-CoV-2 spreads between people through respiratory droplets with a diameter of less than 10 μm and by direct contact.[1–4] It has been shown that wearing masks can significantly reduce the spread of the virus as it limits the distribution of virus containing particles in the room.[5–8] Masks are usually multilayered; each layer has its function (virucidal layer, fluid barrier, particulate filtration layer, etc.),[9–13] and different technological solutions are used to prepare them.[12–15] Since disposable face masks have a limited usage time, the spread of respiratory viruses causes a severe impact on the environment due to the accumulation of disposable face masks, i.e., in 2020, about 129 billion face masks were consumed monthly worldwide.[16–20] Therefore, the development of filter materials for indoor filtration systems with different porosity characteristics (specific surface area, various pore size distribution, pore volume, etc.), good filtration efficiency, and virucidal properties have great potential to limit the spread of the virus in rooms and the impact of used masks on the environment.[21–27] Electrospinning is a versatile method for the production of various filter materials as its process parameters (potential applied, distance between electrodes, solution feed rate, etc.), solution properties (polymer and solvent used, polymer solution concentration and viscosity, etc.), and environment conditions (room temperature and relative humidity) allow to produce materials with different filtering and pore size distribution characteristics.[27–35] It has been shown that variation of different electrospinning process parameters enables the production of materials with various pore sizes (from 0.5 to 500 μm), specific surface areas (up to 50 $m^2\ g^{-1}$), micro-, meso-, and macropore volumes, total pore volumes, and porosities (up to 50%).[31–38] Recent research has shown that nanofiber materials activated with metal (Zn, Ti, Ag, Cu) nanoclusters and compounds have bactericidal[39,40] and virucidal properties; inactivation of various viruses, including poliovirus, HIV-1, coronavirus SARS-CoV-2, and influenza A virus has been demonstrated.[10,25,27,41–53] Several authors have discussed virucidal properties of different metal nanoclusters and ions. The role of silver nanoparticles as the anti-SARS-CoV-2 material has been recently discussed by Arjun et al.[54] and the similar properties of copper-based materials have been discussed by Govind et al.[55] different theories about the mechanisms of said effects have been proposed. For example, it has been theorized that silver nanoparticles interact with biological structures of virions and thus alter their normal functioning while the silver ions are expected to form complexes with electron donor groups of virion molecules.[56] Copper is known to damage virion

[1]Institute of Chemistry, University of Tartu, Ravila 14a, 50411 Tartu, Estonia
[2]Institute of Pharmacy, University of Tartu, Nooruse 1, 50411 Tartu, Estonia
[3]Department of Applied Physics, KTH Royal Institute of Technology, 10691 Stockholm, Sweden
[4]Institute of Physics, University of Tartu, W. Ostwald 1, 50411 Tartu, Estonia
[5]Institute of Ecology and Earth Sciences, University of Tartu, Ravila 14a, 50411 Tartu, Estonia
[6]Institute of Technology, University of Tartu, Nooruse 1, 50411 Tartu, Estonia
[7]Lead contact
*Correspondence: thomas.thomberg@ut.ee
https://doi.org/10.1016/j.isci.2024.109835

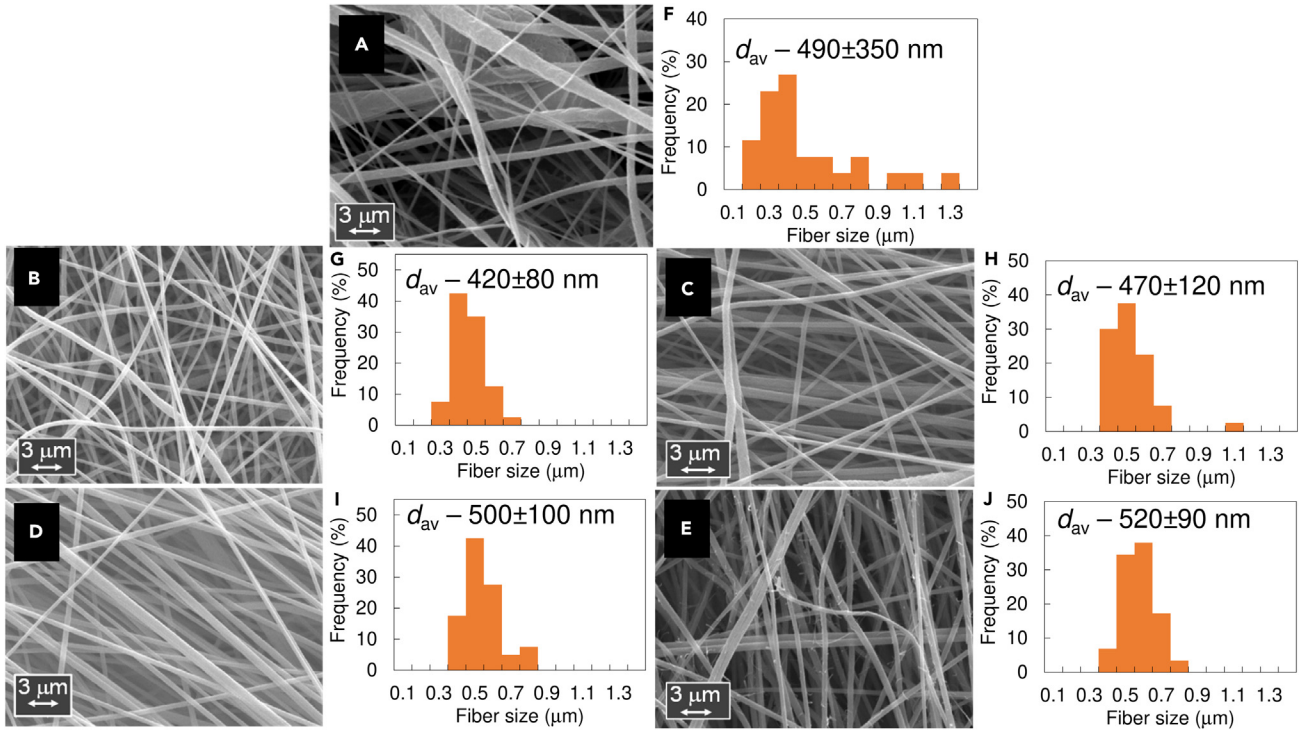

Figure 1. Characterization of materials morphology

(A–E) SEM images and (F–J) fiber diameter distribution plots of electrospun filter materials fabricated using a solution of (A and F) 28 wt % PVDF + DMA at voltage 9 kV and with the addition of *x* wt % $Cu(NO_3)_2 \cdot 2.5H_2O$ at voltage 17 kV (B and G) 0.25 wt %, (C and H) 0.75 wt %, (D and I) 2.0 wt % or (E and J) 3.5 wt %. Scale bars of SEM images (A-E) are shown in the figures.

DNA or RNA. It also interferes with the biological functions of the virion envelope and proteins forming the capsid. Copper is also known to induce the production of reactive oxygen species that can cause the inactivation of virions.[46] Besides virucidal effect the amount of the metal or metal compounds in the material and its influence on the virucidal properties and material stability are significant as well as influencing the adoption of these materials for commercial application.

The aim of this study was to prepare fibrous virucidal filter materials by electrospinning method from the solution of poly(vinylidene difluoride) (PVDF) with the addition of 0.25 wt %, 0.75 wt %, 2.0 wt %, or 3.5 wt % $Cu(NO_3)_2 \cdot 2.5H_2O$. The effect of the preparation parameters on the resulting materials physical characteristics was studied using scanning electron microscopy with energy dispersive X-ray spectroscopy (SEM-EDS), X-ray diffraction (XRD), thermogravimetric analysis (TGA), microwave plasma atomic emission spectroscopy (MP-AES), nitrogen sorption analysis, mercury intrusion porosimetry, and contact angle measurement methods. In order to study the materials filtering properties, the filtering efficiencies were tested against particles of 100, 300, and 3000 nm, and the breathability was established based on pressure drop experiments. Virucidal properties were tested against the SARS-CoV-2 alpha variant, determining the loss of infectivity of the virus in contact with prepared materials; the infectivity of treated samples and controls was analyzed in cell culture using tissue culture infectious dose 50 ($TCID_{50}$) assay.

RESULTS

Physical characterization of electrospun filter materials

SEM analysis was used to characterize the fibrous structure of the electrospun filter materials. All materials containing copper nanoclusters exhibited a uniform and defect-free fibrous structure. The material electrospun from the polymer solution without the addition of copper nanoclusters had a fibrous structure with notable defects (beads) (Figures 1A–1E). The fiber size distribution of the material without the addition of copper nanoclusters was also wider (Figures 1F–1J). Increasing the copper salt concentration in the spinning solution did not significantly affect the fibrous structure of the materials. However, the average fiber diameter increased with $Cu(NO_3)_2 \cdot 2.5H_2O$ concentration in the spinning solution (Figures 1G–1J; Table 1).

The elemental analysis of the electrospun filter materials was performed with SEM-EDS and MP-AES. The peaks in the SEM-EDS spectra (Figure 2A) originate from the used polymer PVDF (C—carbon and F—fluorine) and the copper salt (Cu) as well as from aluminum foil (Al) that was used for collecting deposited electrospun filter material. All mentioned elements are evenly distributed in filter materials as exemplified by SEM-EDS maps measured from filter materials electrospun using a solution of 28 wt % PVDF + DMA with the addition of 2.0 wt %

Table 1. Electrospun filter materials preparation parameters and average fiber diameter d_{av} with a standard deviation

Solution	Voltage (kV)	d_{av} (nm)
28 wt % PVDF + DMA	9	490 ± 350
28 wt % PVDF + DMA +0.25 wt % $Cu(NO_3)_2 \cdot 2.5H_2O$	17	420 ± 80
28 wt % PVDF + DMA +0.75 wt % $Cu(NO_3)_2 \cdot 2.5H_2O$	17	470 ± 120
28 wt % PVDF + DMA +2.0 wt % $Cu(NO_3)_2 \cdot 2.5H_2O$	17	500 ± 100
28 wt % PVDF + DMA +3.5 wt % $Cu(NO_3)_2 \cdot 2.5H_2O$	17	520 ± 90

$Cu(NO_3)_2 \cdot 2.5H_2O$ (Figures 2B–2D). The copper content in the filter materials was determined with SEM-EDS and MP-AES methods (Table 2). The detected copper concentration was very close to the theoretically calculated Cu content. The theoretical Cu content was calculated assuming the complete evaporation of solvent during the electrospinning process and that only salt and polymer remain in the final material.

The crystal structure of the electrospun filter materials was investigated by the XRD method (Figure 3). It revealed that in the case of materials prepared without the addition of $Cu(NO_3)_2 \cdot 2.5H_2O$ in the spinning solution, PVDF was mainly in the gamma form (γ-PVDF, monoclinic structure). In contrast, materials containing copper nanoclusters formed the beta form of PVDF (β-PVDF, orthorhombic structure). The analysis also revealed that in the materials with copper nanoclusters addition, the copper was not present in the form of $Cu(NO_3)_2 \cdot 2.5H_2O$, but as "basic copper nitrate" $Cu_2(NO_3)(OH)_3$, i.e., rouaite.

The thermal stability of electrospun filter materials was investigated by the TGA method. In the inert gas (nitrogen) and synthetic air (20 vol % O_2 and 80 vol % N_2) atmosphere, the main decomposition of all filter materials took place at ~460°C (Figure 4). In the case of materials containing the copper nanoclusters, two small peaks at ~190°C and ~240°C appear in both gas atmospheres. The residual mass for the material prepared using 28 wt % PVDF + DMA +3.5 wt % $Cu(NO_3)_2 \cdot 2.5H_2O$ spinning solution was ~4.2 wt %. The residual mass was substantially higher ~22 wt % for the material prepared without copper salt addition (Figure 4B).

The contact angle values of high purity water on the filter materials were measured to analyze the hydrophilic or hydrophobic properties of the electrospun filter materials (Figure 5). Three repetitive measurements were conducted, but there was no big deviation (±1%) of contact

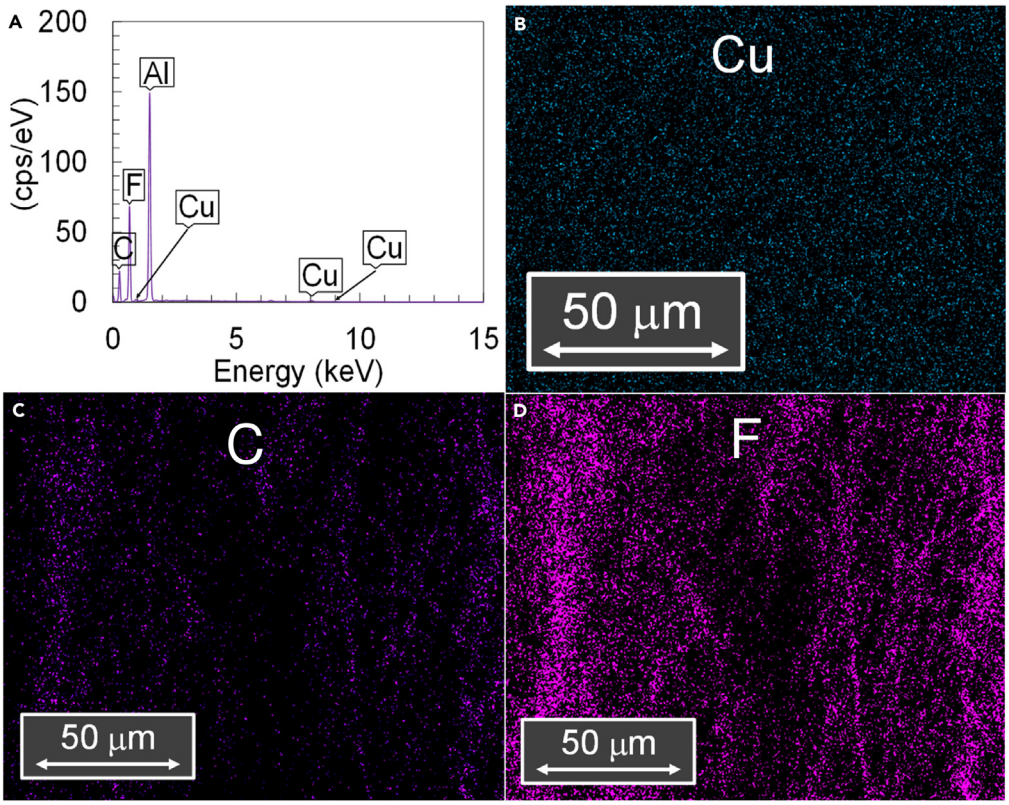

Figure 2. Characterization of materials elemental content and distribution

(A) SEM-EDS spectra and (B–D) SEM-EDS elemental mapping of (B) copper (Cu, light blue), (C) carbon (C, violet) and (D) fluorine (F, pink) of electrospun filter materials fabricated using a solution of 28 wt % PVDF + DMA with the addition of 2.0 wt % $Cu(NO_3)_2 \cdot 2.5H_2O$ at voltage 17 kV. Scale bars of SEM-EDS elemental mapping images (B-D) are shown in the figures.

Table 2. The concentration of copper in electrospun filter materials established by scanning electron microscopy with energy dispersive X-ray spectroscopy (SEM-EDS) and microwave plasma atomic emission spectroscopy (MP-AES) methods compared to theoretical values

Solution	Theoretical (wt %)	SEM-EDS (wt %)	MP-AES (wt %)
28 wt % PVDF + DMA +0.25 wt % $Cu(NO_3)_2 \cdot 2.5H_2O$	0.242	0.22 ± 0.04	0.242 ± 0.001
28 wt % PVDF + DMA +0.75 wt % $Cu(NO_3)_2 \cdot 2.5H_2O$	0.713	0.61 ± 0.08	0.695 ± 0.002
28 wt % PVDF + DMA +2.0 wt % $Cu(NO_3)_2 \cdot 2.5H_2O$	1.82	1.67 ± 0.3	1.750 ± 0.006
28 wt % PVDF + DMA +3.5 wt % $Cu(NO_3)_2 \cdot 2.5H_2O$	3.03	4.05 ± 0.06	2.916 ± 0.02

angle values measured for the same electrospun filter materials under study. All electrospun filter materials were hydrophobic as all contact angles were greater than 90°. The largest wetting angle (146°) was established for the filter material prepared without the copper salt in the spinning solution. The addition of copper salt and the rise of its concentration from 0.25 wt %, 0.75 wt %, 2.0 wt %, to 3.5 wt % in the spinning solution resulted in a decrease of wetting angle from 144°, 138°, 137°–135°, respectively.

Nitrogen sorption analysis and mercury porosimetry measurements were performed to study the prepared materials' porosity (Figure 6; Table 3). The shape of the nitrogen sorption isotherms (Figure 6A) of the electrospun materials can be approximated to isotherm type II according to the IUPAC classification, which describes mainly macroporous materials with little or no microporosity.[57] All copper nanoclusters containing materials have very similar porosities, while slightly higher porosity was observed only for the material without the addition of copper salts in the spinning solution (Figure 6A; Table 3). The mercury intrusion curves (Figure 6B) show several regions with different slopes, describing the gradual filling of pores of various sizes. At low Hg pressures, i.e., the larger pores $D > 10\,000$ nm were filled first, which does not characterize the actual porosity of the material but the voids between the sheets created during the packing of the samples. The mercury intrusion curves (Figure 6B) of electrospun filter materials containing copper nanoclusters show a second slope in the $200 \leq D \leq 5\,000$ nm pore size region. In contrast, the material without nanoclusters has a second slope in the pore size region of $1\,000 \leq D \leq 10\,000$, which implies that later material contains larger pores, and this is illustrated by the pore size distribution pots (Figure 6C). Electrospun filter material prepared without the addition of copper salt in the spinning solution shows a third slope and a peak in pore size distribution plot in the pore size region of $10 \leq D \leq 100$ nm (Figures 6B and 6C) indicating the presence of even smaller pores in this material.

Particle filtration efficiency and pressure drop values for electrospun filter materials

The analysis of the filtration efficiency of electrospun filter materials prepared with the copper salt addition in the spinning solution showed, regardless of their thickness, a high filtration efficiency $E \geq 95\%$ of particles with different sizes (100, 300, and 3000 nm) (Table 4). Conversely, the filter material without copper nanoclusters addition demonstrated high filtration efficiency ($E \geq 99\%$) only for the large particles with a size

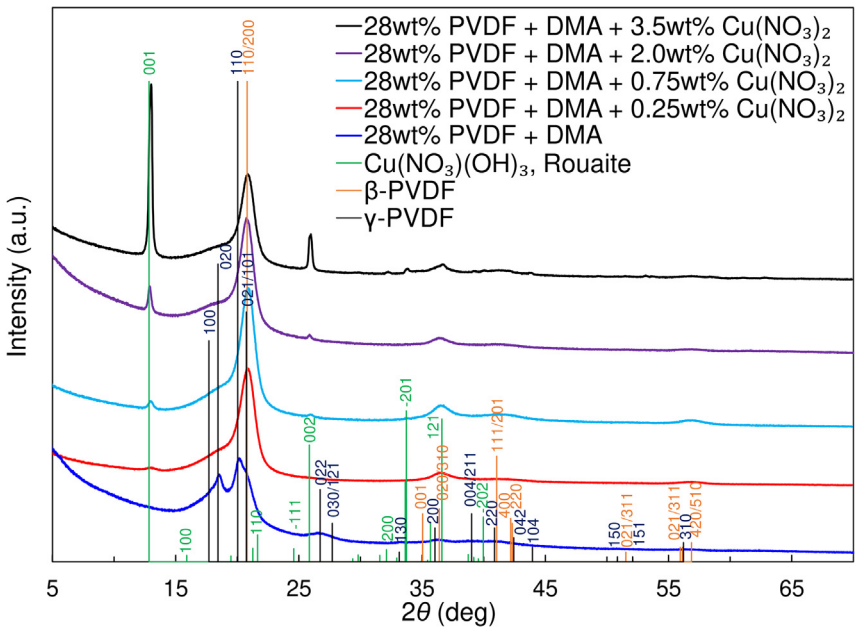

Figure 3. XRD patterns for electrospun filter materials fabricated using a solution of 28 wt % PVDF + DMA at voltage 9 kV and with the addition of x wt % $Cu(NO_3)_2 \cdot 2.5H_2O$ (noted in the figure) at voltage 17 kV

Rouaite, β-PVDF (beta PVDF), and γ-PVDF (gamma PVDF) crystal structure reflections are given as vertical lines for comparison (noted in the figure).

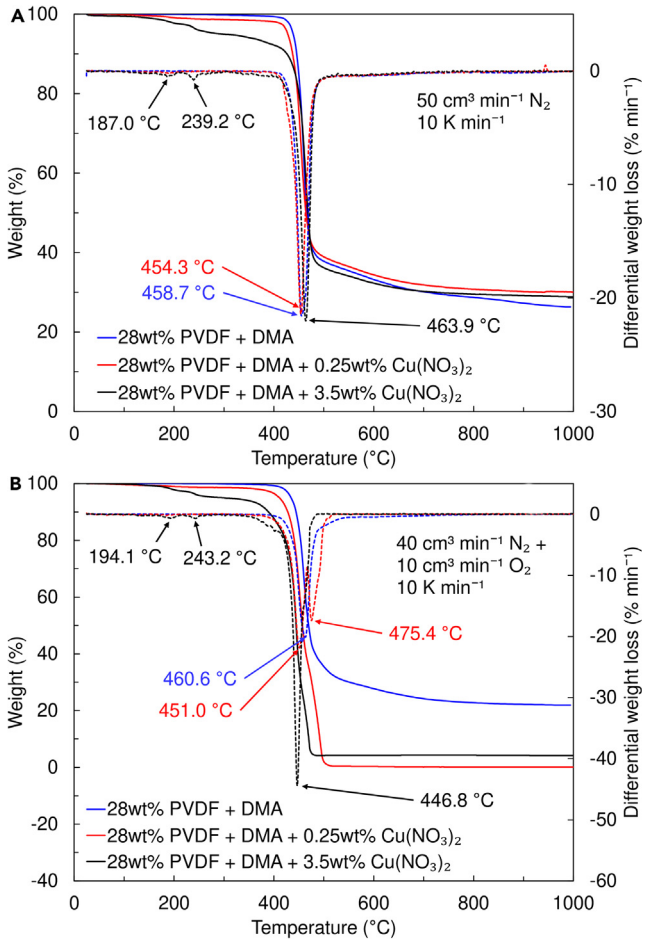

Figure 4. Characterization of materials thermal stability

Thermogravimetric analysis (weight loss—solid line, differential weight loss—dotted lines) in (A) nitrogen and (B) synthetic air (mixture of 20 vol % oxygen and 80 vol % nitrogen) for different electrospun filter materials fabricated using a solution of 28 wt % PVDF + DMA at voltage 9 kV and with the addition of *x* wt % $Cu(NO_3)_2 \cdot 2.5H_2O$ (noted in the figure) at voltage 17 kV.

of 3000 nm. In contrast, the filtration efficiency *E* for particles with a size of 100 and 300 nm was significantly dependent on the material thickness. For example, the filtration efficiency for 130 μm thick material for 300 nm particles was $E \geq 99\%$, while for 55 μm thick material, it was $E \geq 78\%$. For 100 nm particles, the filtration efficiency *E* was even lower and decreased from $E \geq 95\%$ to $E \geq 65\%$ when the material thickness decreased from 130 μm to 55 μm.

Virucidal activity

The virucidal activity of prepared filter materials was tested against SARS-CoV-2. The virucidal activity of the materials fabricated using a spinning solution of 28 wt % PVDF + DMA without the addition of copper salt and with 0.25 wt % or 0.75 wt % $Cu(NO_3)_2 \cdot 2.5H_2O$ were very similar (Figure 7). After a contact time of 12 h the reduction of infectious virus particles $\Delta \log c$ was 0.5 ± 0.05 demonstrating low virucidal activity of all three materials. In sharp contrast, electrospun filter material fabricated with 2.0 wt % or 3.5 wt % copper salt in a spinning solution showed very high virucidal activity. The reduction in viral titer $\Delta \log c$ was 2.5 ± 0.35 and 3.2 ± 0.30 within 12 h, respectively. In the case of the latter material, the decrease in the concentration of infectious virus was also the fastest. For example, within 2 h of contact time, $\Delta \log c$ was 1.7 ± 0.35.

Additionally, the electrospun filter material prepared using 28 wt % PVDF + DMA +2.0 wt % $Cu(NO_3)_2 \cdot 2.5H_2O$ spinning solution demonstrated high stability of virucidal properties over time. The reduction in virus concentration $\Delta \log c$ during a contact time of 8 h was 2.80 ± 0.30 when freshly prepared filter material was tested. The same filter material showed a slight decrease in virus concentration $\Delta \log c$ 2.50 ± 0.45, 2.70 ± 0.30, and 2.40 ± 0.25 after 1, 2, and 3 months of storage, respectively, demonstrating that the virucidal activity of the material did not change significantly, and remained very high even after 3 months.

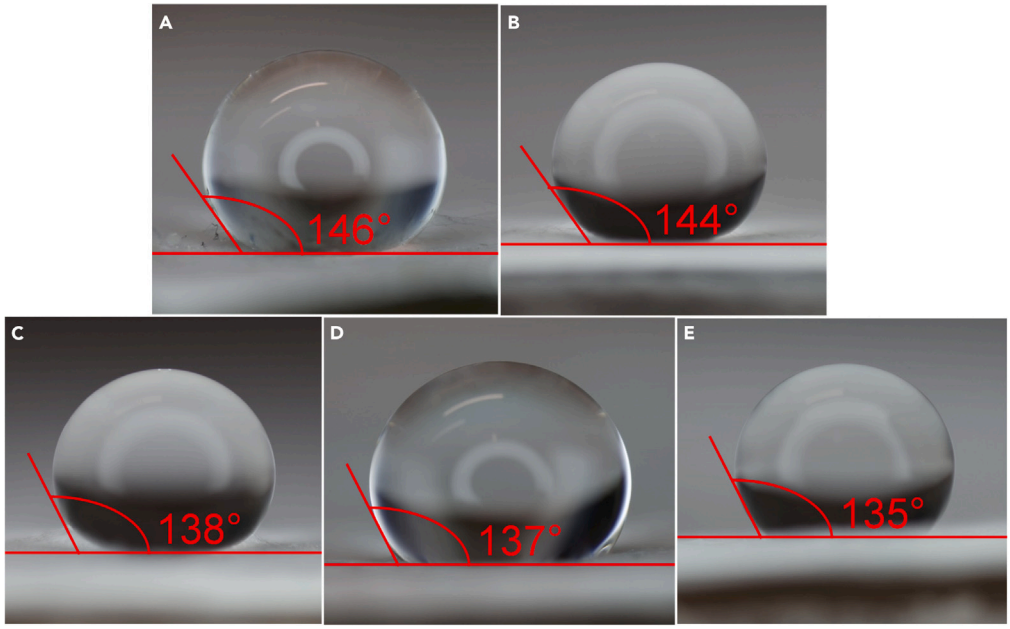

Figure 5. Characterization of materials wetting properties

Microscopic images demonstrating the wetting angle for different electrospun filter materials fabricated using a solution of (A) 28 wt % PVDF + DMA at voltage 9 kV and with the addition of *x* wt % $Cu(NO_3)_2 \cdot 2.5H_2O$ at voltage 17 kV (B) 0.25 wt %, (C) 0.75 wt %, (D) 2.0 wt % or (E) 3.5 wt %.

DISCUSSION

Here, we report the production of filter materials with a virucidal effect. The electrospinning method developed by our research group enables to reproducibly produce materials with suitable fiber structure and diameter, as evidenced by SEM. The smoother appearance of the fibers containing copper nanoparticles is caused by the better conductivity of the spinning solution due to the inclusion of $Cu(NO_3)_2 \cdot 2.5H_2O$. The increase in the mean fiber diameter is probably related to the rise in the electrospun solution viscosity, as the added copper salt contained crystal water, which may cause partial gelation of the PVDF solution.[58] However, the change in the applied voltage did not have a notable effect on the average fiber diameters, as discussed earlier.[45]

The produced materials had uniform copper particle distribution, as evidenced by SEM-EDS. Thus, it supports the conclusion that the electrospinning method is suitable for enriching filter materials with copper and other metal nanoclusters.[27,45] The overall copper content in the filter materials was determined with SEM-EDS and MP-AES methods. While the theoretical values matched with the detected values quite well, the copper content measured with SEM-EDS was higher than expected in the case of sample electrospun using a solution of 28 wt % PVDF + DMA with the addition of 3.5 wt % $Cu(NO_3)_2 \cdot 2.5H_2O$. The semi-quantitative nature of the given method applied can explain this discrepancy.

The solid state form of prepared filter materials was studied with XRD. The obtained results are in good agreement with the literature, where it has been established that PVDF exists in the beta form if it is processed together with metal nanoparticles.[27,45,59,60] The $Cu_2(NO_3)(OH)_3$ that was detected in filter materials is a dehydration product of $Cu(NO_3)_2 \cdot 2.5H_2O$ that is known to form at $\sim 80°C$.[61–63] The increase in intensity of its characteristic XRD peaks at $2\theta \sim 12.9°$ and $2\theta \sim 25.8°$ was correlated with the rise of copper salt concentration in the spinning solution. The peaks corresponding to rouaite are absent in the XRD spectra of the material prepared by drying a portion of the solution in a fume hood and did not undergo the electrospinning process.[27] This suggests that rouaite was formed during the electrospinning process, probably due to the strong electric field applied.

All electrospun filter materials proved to be thermally stable over a wide temperature range, thus being suitable for various filtration applications. The main decomposition of all materials tested corresponds to the decomposition of PVDF.[63–65] In the case of materials containing copper nanoclusters, the two small peaks seen on thermograms measured for copper nanocluster containing materials at ~190°C and ~240°C are due to the decomposition of rouaite into CuO.[27,61,63] The residual mass difference between pure PVDF filter material and PVDF containing rouaite, as detected by TGA, is caused by the nanoparticles catalyzing the decomposition of PVDF.[27,63] In the case of material prepared from a 28 wt % PVDF + DMA +3.5 wt % $Cu(NO_3)_2 \cdot 2.5H_2O$ spinning solution, the residual mass is in good agreement with the theoretical residual mass ~3.95 wt % assuming that the Cu salt is converted to CuO.

The hydrophobic or hydrophilic properties of the prepared materials are essential for capturing virus particles because viruses are often spread using airborne droplets with a diameter of 5–10 μm.[6] The hydrophobicity of the materials decreased with the increase of Cu salt concentration as nanoclusters in fibers.

Since the porosity of the electrospun filter materials is crucial for filtration efficiency, i.e., the capability to capture particles, nitrogen sorption analysis[57,66] and mercury porosimetry measurements[67–69] were performed. All electrospun filter materials proved to be predominantly

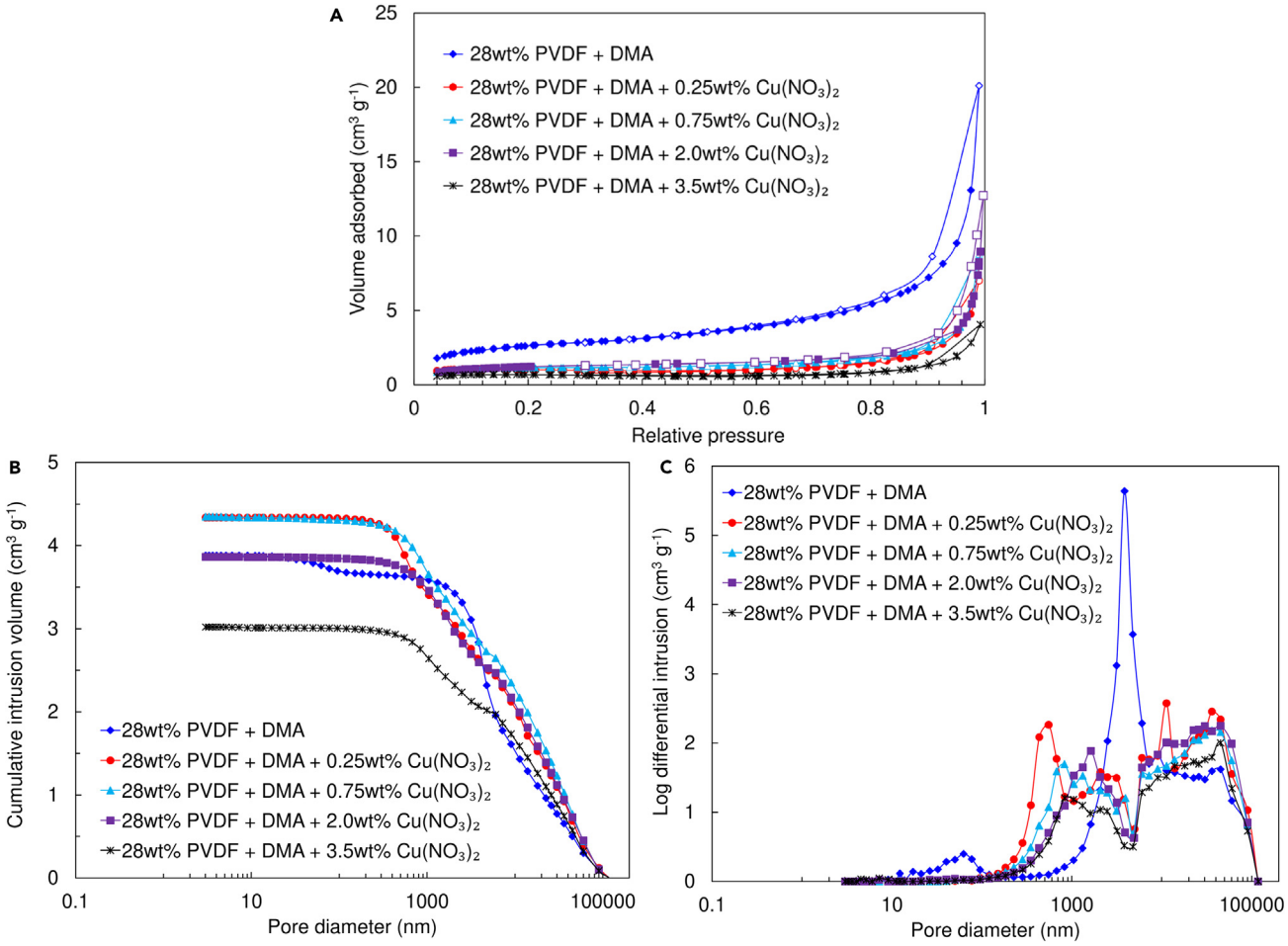

Figure 6. Characterization of materials porosity

(A) Nitrogen sorption isotherms, (B) mercury intrusion curves, and (C) pore size distribution plots obtained from mercury porosimetry data of electrospun filter materials fabricated using a solution of 28 wt % PVDF + DMA at voltage 9 kV and with the addition of *x* wt % $Cu(NO_3)_2 \cdot 2.5H_2O$ (noted in the figure) at voltage 17 kV.

macroporous, and the porosity originates from the inter-fiber voids (Figures 1A–1E). The porosity results given in Table 3 show that the specific surface area S_{Hg}, pore volume V_{Hg}, and overall porosity of the electrospun filter materials are very similar and practically independent of the copper nanocluster content and only material without copper salt nanoclusters addition shows somewhat higher specific surface area S_{Hg}.[27–29,45,70,71]

Measured filtration efficiencies are comparable with previously obtained results.[27,38,45] Furthermore, the results are consistent with the electrospun materials fibrous and porous structure that SEM, nitrogen sorption, and mercury porosimetry revealed. The methods showed that the fibers are more closely spaced in the case of the materials prepared with copper salt addition in a spinning solution (Figures 1B–1E) and have smaller pores in the $200 \leq D \leq 5\,000$ nm size range. Smaller pores ensure better filtration efficiency of materials with copper nanoclusters addition (Table 4) compared to the material without copper nanoclusters addition, which have prominent pores in the size range of $1000 \leq D \leq 10\,000$ nm (Figure 6C). Additionally, it can be noted that the pressure drop and hence the breathability depends significantly and approximately linearly on the thickness of the materials (Table 4).

The virucidal activity of tested materials did not change over time, thus confirming their suitability for use as filter materials. Virucidal activity testing revealed that the effect is concentration dependent. While the reduction of infectious virions Δlogc was detectable after 12 h contact time with the filter materials prepared with the addition of 0.25 wt % or 0.75 wt % $Cu(NO_3)_2 \cdot 2.5H_2O$, it was comparable to the virucidal activity of the materials fabricated using a spinning solution of 28 wt % PVDF + DMA without the addition of copper salt. The filter material prepared with the highest copper concentration proved also to have the highest virucidal activity. At the same time, the filter material with the second highest copper content showed a marked effect compared to the material without copper. It is possible that only the copper nanoclusters on the surface of the fibers affect virions. Obviously, the amount of nanoclusters on the fiber surface depends on the spinning solution's overall salt content. Thus, the virucidic effect appears only in a significant manner when there is enough copper containing

Table 3. The specific surface area (S_{BET}) calculated by Brunauer-Emmett-Teller (BET) theory and total pore volume (V_{sum}) from nitrogen sorption and specific surface area S_{Hg}, pore volume V_{Hg}, and porosity from mercury intrusion measurements for electrospun filter materials fabricated using a solution of 28 wt % PVDF + DMA without and with the addition of *x* wt % $Cu(NO_3)_2 \cdot 2.5H_2O$

	Nitrogen sorption		Mercury intrusion		
Solution	S_{BET} ($m^2\ g^{-1}$)	V_{tot} ($cm^3\ g^{-1}$)	S_{Hg} ($m^2\ g^{-1}$)	V_{Hg} ($cm^3\ g^{-1}$)	Porosity (%)
28 wt % PVDF + DMA	9.6	0.015	23.5	3.88	28.2
28 wt % PVDF + DMA +0.25 wt % $Cu(NO_3)_2 \cdot 2.5H_2O$	3.6	0.0057	10.3	4.34	25.9
28 wt % PVDF + DMA +0.75 wt % $Cu(NO_3)_2 \cdot 2.5H_2O$	4.3	0.0060	7.5	3.82	28.6
28 wt % PVDF + DMA +2.0 wt % $Cu(NO_3)_2 \cdot 2.5H_2O$	4.4	0.0057	8.1	3.87	27.1
28 wt % PVDF + DMA +3.5 wt % $Cu(NO_3)_2 \cdot 2.5H_2O$	2.5	0.0034	10.9	3.02	31.5

particles present on the surface. The virucidal activity of copper compounds against SARS-CoV-2 has also been observed in other recently published papers, where the effect of different metal nanoparticles on the SARS-CoV-2 virus has been investigated.[27,44,72]

Conclusions

Electrospinning enabled the manufacture of filter materials based on poly(vinylidene difluoride) (PVDF) with different copper nanoparticle concentrations. The electrospun filter materials' fiber morphology, elemental composition, crystal structure, thermal stability, porosity, wettability, filtration and virucidal properties were suitable for air filtration purposes. Electrospun filter materials fabricated with the addition of $Cu(NO_3)_2 \cdot 2.5H_2O$ in the spinning solution had fewer defects, and their fibers were more uniformly distributed than those produced without copper nanocluster content. An increase of $Cu(NO_3)_2 \cdot 2.5H_2O$ concentration in the spinning solution resulted in an increase in average fiber diameter that could be caused by gelation of the polymer solution due to crystal water in copper salt. Electrospun filter materials contained mainly carbon, fluor, and copper, evenly distributed across the materials. The PVDF was in the gamma form in filter materials fabricated from solution without the addition of the copper salt. In contrast, the beta form of PVDF was observed in filter materials with copper nanoclusters content. The copper was in the form of $Cu_2(NO_3)(OH)_3$ in the materials manufactured with electrospinning. This is a dehydration product of $Cu(NO_3)_2 \cdot 2.5H_2O$, and it probably forms during the electrospinning process due to the high electric field strength applied. The electrospun filter materials were generally thermally stable. All the electrospun filter materials were very hydrophobic as the wetting angles varied from 135° to 146°. The materials became less hydrophobic with increased $Cu(NO_3)_2 \cdot 2.5H_2O$ concentration in the spinning solution. Most of the pores in filter materials fabricated without the addition of the copper salt were larger ($1000 \leq D \leq 10\,000$ nm) than most of the pores in materials with the copper salt addition ($200 \leq D \leq 5\,000$ nm). However, the total porosity was nearly similar for all fabricated materials.

All electrospun filter materials with an addition of $Cu(NO_3)_2 \cdot 2.5H_2O$ in the spinning solution showed high filtration efficiency of particles in different sizes (100, 300, and 3000 nm) regardless of the thickness of the material or added copper salt content. Materials without the copper nanoclusters' content had generally lower filtration efficiency. Electrospun filter materials fabricated with high $Cu(NO_3)_2 \cdot 2.5H_2O$ content, i.e., 2.0 wt % and 3.5 wt % in a spinning solution exhibited significant virucidal properties. During a contact time of 12 h the reduction of infectious virus particles $\Delta\log c$ was 2.5 ± 0.35 and 3.2 ± 0.30, respectively. The fastest reduction in infectious virion concentration occurred when the

Table 4. Particle filtration efficiency (*E*) and pressure drop of electrospun filter materials with various thicknesses fabricated using a solution of 28 wt % PVDF + DMA at voltage 9 kV and with the addition of *x* wt % $Cu(NO_3)_2 \cdot 2.5H_2O$ (noted in Table) at voltage 17 kV

Solution	Filter thickness (μm)	*E*, 100 nm (%)	*E*, 300 nm (%)	*E*, 3000 nm (%)	Pressure drop ($Pa\ cm^{-2}$)
28 wt % PVDF + DMA	55 ± 5	65.3 ± 1.2	75.9 ± 0.1	99.5 ± 0.1	53 ± 6
	85 ± 5	83.9 ± 4.1	92.4 ± 1.8	99.9 ± 0.1	51.3 ± 5
	130 ± 8	95.5 ± 1.1	99.2 ± 0.2	99.9 ± 0.0	144.3 ± 12
28 wt % PVDF + DMA +0.75 wt % $Cu(NO_3)_2 \cdot 2.5H_2O$	25 ± 3	100 ± 0.0	100 ± 0.0	100 ± 0.0	128 ± 2
	100 ± 10	100 ± 0.0	100 ± 0.0	100 ± 0.0	456 ± 10
	200 ± 20	100 ± 0.0	100 ± 0.0	100 ± 0.0	819 ± 52
28 wt % PVDF + DMA +2.0 wt % $Cu(NO_3)_2 \cdot 2.5H_2O$	35 ± 4	98.5 ± 0.5	99.7 ± 0.2	100 ± 0.3	106 ± 2
	90 ± 8	100 ± 0.0	100 ± 0.1	100 ± 0.0	387 ± 86
	145 ± 10	99.9 ± 0.1	99.9 ± 0.1	99.9 ± 0.1	693 ± 74
28 wt % PVDF + DMA +3.5 wt % $Cu(NO_3)_2 \cdot 2.5H_2O$	30 ± 5	95.4 ± 3.8	100 ± 0.0	100 ± 0.0	86 ± 16
	110 ± 15	100 ± 0.0	100 ± 0.0	100 ± 0.0	143 ± 12
	200 ± 20	100 ± 0.0	100 ± 0.0	100 ± 0.0	400 ± 97

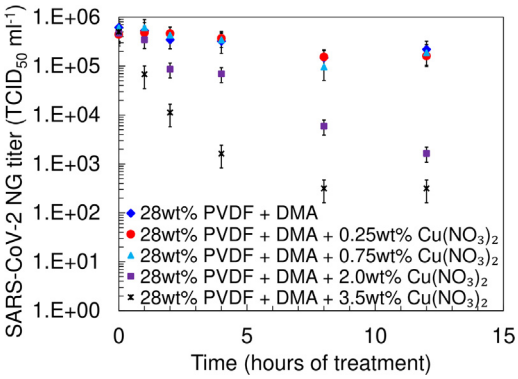

Figure 7. Virucidal activity against SARS-CoV-2 of electrospun filter materials fabricated using a solution of 28 wt % PVDF + DMA at voltage 9 kV and with the addition of *x* wt % $Cu(NO_3)_2 \cdot 2.5H_2O$ (noted in the figure) at voltage 17 kV

Data are represented as mean with standard deviation.

material fabricated from a spinning solution containing 3.5 wt % of $Cu(NO_3)_2 \cdot 2.5H_2O$ was used. In contrast, electrospun filter materials with low $Cu(NO_3)_2 \cdot 2.5H_2O$ content ($\leq$0.75 wt %) in the spinning solution did not show remarkable virucidal activity. The electrospun filter material prepared using 28 wt % PVDF + DMA +2.0 wt % $Cu(NO_3)_2 \cdot 2.5H_2O$ spinning solution demonstrated high virucidal stability even 3 months after the material was prepared.

Limitations of the study

While we have shown excellent performance of our materials in laboratory settings, testing the efficiency of produced materials in practical environments would be vital. It is also necessary to study given materials' effectiveness in operando. Furthermore, it is required to challenge provided materials with various conditions to test their stability in different operating environments.

STAR★METHODS

Detailed methods are provided in the online version of this paper and include the following:

- KEY RESOURCES TABLE
- RESOURCE AVAILABILITY
  - Lead contact
  - Materials availability
  - Data and code availability
- METHOD DETAILS
  - Spinning solution preparation
  - Electrospun filter materials preparation
  - Physical characterization of electrospun filter materials
  - Electrospun filter materials particle filtration efficiency and breathability
  - Virus strain and virucidal activity determination

ACKNOWLEDGMENTS

This research was supported by the EU through the European Regional Development Fund under project TK141, "Advanced materials and high-technology devices for energy recuperation systems" (2014–2020.4.01.15–0011) and TK210, "Estonian Centre of Excellence in Green Hydrogen and Sustainable Energetics", and by the Estonian Research Council (projects no. IUT 20-13, IUT20-27, MOBTT42, PRG676, PRG714, and COVSG36). KTH acknowledges funding from the Ragnar Holm Foundation, the Swedish Research Council (VR, Dnr. 2021-06157 and Dnr. 2022-03936), the Swedish Foundation for Strategic Research (SSF, SwedNess), and the Carl Tryggers Foundation for Scientific Research (CTS-22:2374). Finally, we are thankful to the Department of Chemical Engineering, KTH, Sweden, for granting access to the Hg porosimetry instrument and for giving technical assistance and support during the measurements.

AUTHOR CONTRIBUTIONS

Conceptualization, T.T., A.L., and E.L.; methodology, H.B., T.T., A.L., and E.L.; validation, H.B., T.T., J.N., M. Koppel., R.P., M.V., P.P., and M.P.; formal analysis, H.B., T.T., M.V., P.P. and M.P.; investigation, H.B., T.T., J.N., M Koppel., T.R., R.P., M.V., P.P., and M.P.; resources, T.T., J.N., M. Koppel., T.R., M.M., H.J., M. Külaviir., P.P., K.K., M.P., L.V., A.M., and E.L.; writing – original draft, H.B., T.T., A.L., J.N., R.P., H.J., P.P., M.P., and L.V.; writing – review and editing, H.B., T.T., A.L., R.P., M.M., H.J., K.K., M.P., L.V., A.M., and E.L.; visualization, H.B., T.T., J.N., M. Koppel, T.R., R.P., M. Külaviir., and M.P.; supervision, T.T., M.M., H.J., K.K., L.V., A.M., and E.L.; project administration, T.T., M.M., H.J., K.K., A.M., and E.L.; funding acquisition, M.M., H.J., K.K., A.M., and E.L.

DECLARATION OF INTERESTS

The authors declare no conflict of interest.

Received: December 29, 2023
Revised: April 11, 2024
Accepted: April 25, 2024
Published: April 27, 2024

REFERENCES

1. Lee, E.C., Wada, N.I., Grabowski, M.K., Gurley, E.S., and Lessler, J. (2020). The engines of SARS-CoV-2 spread. Science *370*, 406–407. https://doi.org/10.1126/science.abd8755.
2. Pivato, A., Amoruso, I., Formenton, G., Di Maria, F., Bonato, T., Vanin, S., Marion, A., and Baldovin, T. (2021). Evaluating the presence of SARS-CoV-2 RNA in the particulate matters during the peak of COVID-19 in Padua, northern Italy. Sci. Total Environ. *784*, 147129. https://doi.org/10.1016/j.scitotenv.2021.147129.
3. Babaahmadi, V., Amid, H., Naeimirad, M., and Ramakrishna, S. (2021). Biodegradable and multifunctional surgical face masks: A brief review on demands during COVID-19 pandemic, recent developments, and future perspectives. Sci. Total Environ. *798*, 149233. https://doi.org/10.1016/j.scitotenv.2021.149233.
4. Wang, C.C., Prather, K.A., Sznitman, J., Jimenez, J.L., Lakdawala, S.S., Tufekci, Z., and Marr, L.C. (2021). Airborne transmission of respiratory viruses. Science *373*, eabd9149. https://doi.org/10.1126/science.abd9149.
5. Cook, T.M. (2020). Personal protective equipment during the coronavirus disease (COVID) 2019 pandemic – a narrative review. Anaesthesia *75*, 920–927. https://doi.org/10.1111/anae.15071.
6. Prather, K.A., Wang, C.C., and Schooley, R.T. (2020). Reducing transmission of SARS-CoV-2. Science *368*, 1422–1424. https://doi.org/10.1126/science.abc6197.
7. Cui, J., Li, F., and Shi, Z.-L. (2019). Origin and evolution of pathogenic coronaviruses. Nat. Rev. Microbiol. *17*, 181–192. https://doi.org/10.1038/s41579-018-0118-9.
8. Cheng, V.C.-C., Wong, S.-C., Chuang, V.W.-M., So, S.Y.-C., Chen, J.H.-K., Sridhar, S., To, K.K.-W., Chan, J.F.-W., Hung, I.F.-N., Ho, P.-L., and Yuen, K.Y. (2020). The role of community-wide wearing of face mask for control of coronavirus disease 2019 (COVID-19) epidemic due to SARS-CoV-2. J. Infect. *81*, 107–114. https://doi.org/10.1016/j.jinf.2020.04.024.
9. Rahman, M.Z., Hoque, M.E., Alam, M.R., Rouf, M.A., Khan, S.I., Xu, H., and Ramakrishna, S. (2022). Face Masks to Combat Coronavirus (COVID-19)—Processing, Roles, Requirements, Efficacy, Risk and Sustainability. Polymers *14*, 1296. https://doi.org/10.3390/polym14071296.
10. Deng, W., Sun, Y., Yao, X., Subramanian, K., Ling, C., Wang, H., Chopra, S.S., Xu, B.B., Wang, J.-X., Chen, J.-F., et al. (2022). Masks for COVID-19. Adv. Sci. *9*, 2102189. https://doi.org/10.1002/advs.202102189.
11. Ganesapillai, M., Mondal, B., Sarkar, I., Sinha, A., Ray, S.S., Kwon, Y.-N., Nakamura, K., and Govardhan, K. (2022). The face behind the Covid-19 mask — A comprehensive review. Environ. Technol. Innov. *28*, 102837. https://doi.org/10.1016/j.eti.2022.102837.
12. Chua, M.H., Cheng, W., Goh, S.S., Kong, J., Li, B., Lim, J.Y.C., Mao, L., Wang, S., Xue, K., Yang, L., et al. (2020). Face Masks in the New COVID-19 Normal: Materials, Testing, and Perspectives. Research *2020*, 7286735. https://doi.org/10.34133/2020/7286735.
13. Wibisono, Y., Fadila, C.R., Saiful, S., and Bilad, M.R. (2020). Facile Approaches of Polymeric Face Masks Reuse and Reinforcements for Micro-Aerosol Droplets and Viruses Filtration: A Review. Polymers *12*, 2516. https://doi.org/10.3390/polym12112516.
14. Teo, J.Y., Kng, J., Periaswamy, B., Liu, S., Lim, P.C., Lee, C.E., Tan, B.H., Loh, X.J., Ni, X., Tiang, D., et al. (2021). Exploring Reusability of Disposable Face Masks: Effects of Disinfection Methods on Filtration Efficiency, Breathability, and Fluid Resistance. Glob. Chall. *5*, 2100030. https://doi.org/10.1002/gch2.202100030.
15. Rubio-Romero, J.C., Pardo-Ferreira, M.D.C., Torrecilla-García, J.A., and Calero-Castro, S. (2020). Disposable masks: Disinfection and sterilization for reuse, and non-certified manufacturing, in the face of shortages during the COVID-19 pandemic. Saf. Sci. *129*, 104830. https://doi.org/10.1016/j.ssci.2020.104830.
16. Hui Li, A.S., Sathishkumar, P., Selahuddeen, M.L., Asyraf Wan Mahmood, W.M., Zainal Abidin, M.H., Wahab, R.A., Mohamed Huri, M.A., and Abdullah, F. (2022). Adverse environmental effects of disposable face masks due to the excess usage. Environ. Pollut. *308*, 119674. https://doi.org/10.1016/j.envpol.2022.119674.
17. Du, H., Huang, S., and Wang, J. (2022). Environmental risks of polymer materials from disposable face masks linked to the COVID-19 pandemic. Sci. Total Environ. *815*, 152980. https://doi.org/10.1016/j.scitotenv.2022.152980.
18. Atılgan Türkmen, B. (2022). Life cycle environmental impacts of disposable medical masks. Environ. Sci. Pollut. Res. *29*, 25496–25506. https://doi.org/10.1007/s11356-021-17430-5.
19. Liu, R., and Mabury, S.A. (2021). Single-Use Face Masks as a Potential Source of Synthetic Antioxidants to the Environment. Environ. Sci. Technol. Lett. *8*, 651–655. https://doi.org/10.1021/acs.estlett.1c00422.
20. Prata, J.C., Silva, A.L.P., Walker, T.R., Duarte, A.C., and Rocha-Santos, T. (2020). COVID-19 Pandemic Repercussions on the Use and Management of Plastics. Environ. Sci. Technol. *54*, 7760–7765. https://doi.org/10.1021/acs.est.0c02178.
21. Chang, S.-Y., Huang, K.-Y., Chao, T.-L., Kao, H.-C., Pang, Y.-H., Lu, L., Chiu, C.-L., Huang, H.-C., Cheng, T.-J.R., Fang, J.-M., and Yang, P.C. (2021). Nanoparticle composite TPNT1 is effective against SARS-CoV-2 and influenza viruses. Sci. Rep. *11*, 8692. https://doi.org/10.1038/s41598-021-87254-3.
22. Gopal, V., Nilsson-Payant, B.E., French, H., Siegers, J.Y., Yung, W.S., Hardwick, M., and Te Velthuis, A.J.W. (2021). Zinc-embedded polyamide fabrics inactivate SARS-CoV-2 and influenza A virus. ACS Appl. Mater. Interfaces *13*, 30317–30325. https://doi.org/10.1021/acsami.1c04412.
23. Joe, Y.H., Woo, K., and Hwang, J. (2014). Fabrication of an anti-viral air filter with SiO2–Ag nanoparticles and performance evaluation in a continuous airflow condition. J. Hazard Mater. *280*, 356–363. https://doi.org/10.1016/j.jhazmat.2014.08.013.
24. Kim, S., Chung, J., Lee, S.H., Yoon, J.H., Kweon, D.-H., and Chung, W.-J. (2021). Tannic acid-functionalized HEPA filter materials for influenza virus capture. Sci. Rep. *11*, 979. https://doi.org/10.1038/s41598-020-78929-4.
25. Mallakpour, S., Azadi, E., and Hussain, C.M. (2022). Fabrication of air filters with advanced filtration performance for removal of viral aerosols and control the spread of COVID-19. Adv. Colloid Interface Sci. *303*, 102653. https://doi.org/10.1016/j.cis.2022.102653.
26. Lee, J., Bae, J., Youn, D.-Y., Ahn, J., Hwang, W.-T., Bae, H., Bae, P.K., and Kim, I.-D. (2022). Violacein-embedded nanofiber filters with antiviral and antibacterial activities. Chem. Eng. J. *444*, 136460. https://doi.org/10.1016/j.cej.2022.136460.
27. Thomberg, T., Bulgarin, H., Lust, A., Nerut, J., Koppel, M., Romann, T., Palm, R., Månsson, M., Flores March, N.M., Junninen, H., et al. (2023). The anti SARS-CoV-2 activity of nanofibrous filter materials activated with metal clusters. Atmos. Environ. X *17*, 100212. https://doi.org/10.1016/j.aeaoa.2023.100212.
28. Tõnurist, K., Jänes, A., Thomberg, T., Kurig, H., and Lust, E. (2009). Influence of mesoporous separator properties on the parameters of electrical double-layer capacitor single cells. J. Electrochem. Soc. *156*, A334–A342.
29. Tõnurist, K., Thomberg, T., Jänes, A., and Lust, E. (2013). Specific performance of supercapacitors at lower temperatures based on different separator materials. J. Electrochem. Soc. *160*, A449–A457. https://doi.org/10.1149/2.044303jes.
30. Tõnurist, K., Vaas, I., Thomberg, T., Jänes, A., Kurig, H., Romann, T., and Lust, E. (2014). Application of multistep electrospinning method for preparation of electrical double-layer capacitor half-cells. Electrochim. Acta *119*, 72–77. https://doi.org/10.1016/j.electacta.2013.11.155.
31. Mamun, A., Blachowicz, T., and Sabantina, L. (2021). Electrospun nanofiber mats for filtering applications—technology, structure and materials. Polymers *13*, 1368. https://doi.org/10.3390/polym13091368.

32. Sundarrajan, S., Tan, K.L., Lim, S.H., and Ramakrishna, S. (2014). Electrospun Nanofibers for Air Filtration Applications. Procedia Eng. *75*, 159–163. https://doi.org/10.1016/j.proeng.2013.11.034.
33. Lu, T., Cui, J., Qu, Q., Wang, Y., Zhang, J., Xiong, R., Ma, W., and Huang, C. (2021). Multistructured Electrospun Nanofibers for Air Filtration: A Review. ACS Appl. Mater. Interfaces *13*, 23293–23313. https://doi.org/10.1021/acsami.1c06520.
34. Senthil, R., Sumathi, V., Tamilselvi, A., Kavukcu, S.B., and Aruni, A.W. (2022). Functionalized electrospun nanofibers for high efficiency removal of particulate matter. Sci. Rep. *12*, 8411. https://doi.org/10.1038/s41598-022-12505-w.
35. Borojeni, I.A., Gajewski, G., and Riahi, R.A. (2022). Application of Electrospun Nonwoven Fibers in Air Filters. Fibers *10*, 15. https://doi.org/10.3390/fib10020015.
36. Xu, X., Yang, Q., Wang, Y., Yu, H., Chen, X., and Jing, X. (2006). Biodegradable electrospun poly(l-lactide) fibers containing antibacterial silver nanoparticles. Eur. Polym. J. *42*, 2081–2087. https://doi.org/10.1016/j.eurpolymj.2006.03.032.
37. Neisiany, R.E., Enayati, M.S., Kazemi-Beydokhti, A., Das, O., and Ramakrishna, S. (2020). Multilayered bio-based electrospun membranes: A potential porous media for filtration applications. Front. Mater. *7*, 67. https://doi.org/10.3389/fmats.2020.00067.
38. Karabulut, F.N.H., Höfler, G., Ashok Chand, N., and Beckermann, G.W. (2021). Electrospun nanofibre filtration media to protect against biological or nonbiological airborne particles. Polymers *13*, 3257. https://doi.org/10.3390/polym13193257.
39. Bondarenko, O., Juganson, K., Ivask, A., Kasemets, K., Mortimer, M., and Kahru, A. (2013). Toxicity of Ag, CuO and ZnO nanoparticles to selected environmentally relevant test organisms and mammalian cells *in vitro*: a critical review. Arch. Toxicol. *87*, 1181–1200. https://doi.org/10.1007/s00204-013-1079-4.
40. Ivask, A., Juganson, K., Bondarenko, O., Mortimer, M., Aruoja, V., Kasemets, K., Blinova, I., Heinlaan, M., Slaveykova, V., and Kahru, A. (2014). Mechanisms of toxic action of Ag, ZnO and CuO nanoparticles to selected ecotoxicological test organisms and mammalian cells *in vitro*: A comparative review. Nanotoxicology *8*, 57–71. https://doi.org/10.3109/17435390.2013.855831.
41. Sundberg, A., Champagne, V., McNally, B., Helfritch, D., and Sisson, R. (2015). Effectiveness of nanomaterial copper cold spray surfaces on inactivation of influenza A virus. J. Biotechnol. Biomater. *5*, 205. https://doi.org/10.4172/2155-952X.1000205.
42. Qamar, H., Rehman, S., Chauhan, D.K., Tiwari, A.K., and Upmanyu, V. (2020). Green synthesis, characterization and antimicrobial activity of copper oxide nanomaterial derived from momordica charantia. Int. J. Nanomed. *15*, 2541–2553. https://doi.org/10.2147/IJN.S240232.
43. Tavakoli, A., and Hashemzadeh, M.S. (2020). Inhibition of herpes simplex virus type 1 by copper oxide nanoparticles. J. Virol. Methods *275*, 113688. https://doi.org/10.1016/j.jviromet.2019.113688.
44. Kubo, A.-L., Rausalu, K., Savest, N., Žusinaite, E., Vasiliev, G., Viirsalu, M., Plamus, T., Krumme, A., Merits, A., and Bondarenko, O. (2022). Antibacterial and Antiviral Effects of Ag, Cu and Zn Metals, Respective Nanoparticles and Filter Materials Thereof against Coronavirus SARS-CoV-2 and Influenza A Virus. Pharmaceutics *14*, 2549. https://doi.org/10.3390/pharmaceutics14122549.
45. Thomberg, T., Ramah, P., Lust, A., Nerut, J., Koppel, M., Romann, T., Palm, R., Månsson, M., March, N.F., Junninen, H., et al. (2022). Preparation of nanofibrous materials activated with metal clusters for active and long-lasting air filters. Separ. Purif. Technol. *288*, 120697. https://doi.org/10.1016/j.seppur.2022.120697.
46. Bahrami, A., Arabestani, M.R., Taheri, M., Farmany, A., Norozzadeh, F., Hosseini, S.M., Nozari, H., and Nouri, F. (2022). Exploring the Role of Heavy Metals and Their Derivatives on the Pathophysiology of COVID-19. Biol. Trace Elem. Res. *200*, 2639–2650. https://doi.org/10.1007/s12011-021-02893-x.
47. Jeremiah, S.S., Miyakawa, K., Morita, T., Yamaoka, Y., and Ryo, A. (2020). Potent antiviral effect of silver nanoparticles on SARS-CoV-2. Biochem. Biophys. Res. Commun. *533*, 195–200. https://doi.org/10.1016/j.bbrc.2020.09.018.
48. Xiang, D.x., Chen, Q., Pang, L., and Zheng, C.l. (2011). Inhibitory effects of silver nanoparticles on H1N1 influenza A virus *in vitro*. J. Virol. Methods *178*, 137–142. https://doi.org/10.1016/j.jviromet.2011.09.003.
49. Fujimori, Y., Sato, T., Hayata, T., Nagao, T., Nakayama, M., Nakayama, T., Sugamata, R., and Suzuki, K. (2012). Novel Antiviral Characteristics of Nanosized Copper(I) Iodide Particles Showing Inactivation Activity against 2009 Pandemic H1N1 Influenza Virus. Appl. Environ. Microbiol. *78*, 951–955. https://doi.org/10.1128/AEM.06284-11.
50. Maduray, K., and Parboosing, R. (2021). Metal Nanoparticles: a Promising Treatment for Viral and Arboviral Infections. Biol. Trace Elem. Res. *199*, 3159–3176. https://doi.org/10.1007/s12011-020-02414-2.
51. Toledo, G.G.D., Toledo, V.H., Lanfredi, A.J.C., Escote, M., Champi, A., Silva, M.C.C.D., and Nantes-Cardoso, I.L. (2020). Promising Nanostructured Materials against Enveloped Virus. An. Acad. Bras. Cienc. *92*, e20200718. https://doi.org/10.1590/0001-3765202020200718.
52. Aallaei, M., Molaakbari, E., Mostafavi, P., Salarizadeh, N., Maleksah, R.E., and Afzali, D. (2022). Investigation of Cu metal nanoparticles with different morphologies to inhibit SARS-CoV-2 main protease and spike glycoprotein using Molecular Docking and Dynamics Simulation. J. Mol. Struct. *1253*, 132301. https://doi.org/10.1016/j.molstruc.2021.132301.
53. Rani, I., Goyal, A., Bhatnagar, M., Manhas, S., Goel, P., Pal, A., and Prasad, R. (2021). Potential molecular mechanisms of zinc- and copper-mediated antiviral activity on COVID-19. Nutr. Res. *92*, 109–128. https://doi.org/10.1016/j.nutres.2021.05.008.
54. Arjun, P.N.J., Sankar, B., Shankar, K.V., Kulkarni, N.V., Sivasankaran, S., and Shankar, B. (2022). Silver and Silver Nanoparticles for the Potential Treatment of COVID-19: A Review. Coatings *12*, 1679. https://doi.org/10.3390/coatings12111679.
55. Govind, V., Bharadwaj, S., Sai Ganesh, M.R., Vishnu, J., Shankar, K.V., Shankar, B., and Rajesh, R. (2021). Antiviral properties of copper and its alloys to inactivate covid-19 virus: a review. Biometals *34*, 1217–1235. https://doi.org/10.1007/s10534-021-00339-4.
56. Galdiero, S., Falanga, A., Vitiello, M., Cantisani, M., Marra, V., and Galdiero, M. (2011). Silver Nanoparticles as Potential Antiviral Agents. Molecules *16*, 8894–8918. https://doi.org/10.3390/molecules16108894.
57. Thommes, M., Kaneko, K., Neimark, A.V., Olivier, J.P., Rodriguez-Reinoso, F., Rouquerol, J., and Sing, K.S. (2015). Physisorption of gases, with special reference to the evaluation of surface area and pore size distribution (IUPAC Technical Report). Pure Appl. Chem. *87*, 1051–1069. https://doi.org/10.1515/pac-2014-1117.
58. Marshall, J.E., Zhenova, A., Roberts, S., Petchey, T., Zhu, P., Dancer, C.E.J., McElroy, C.R., Kendrick, E., and Goodship, V. (2021). On the solubility and stability of polyvinylidene fluoride. Polymers *13*, 1354. https://doi.org/10.3390/polym13091354.
59. Wang, W., Zhang, S., Srisombat, L.O., Lee, T.R., and Advincula, R.C. (2011). Gold-nanoparticle- and gold-nanoshell-induced polymorphism in poly(vinylidene fluoride). Macromol. Mater. Eng. *296*, 178–184. https://doi.org/10.1002/mame.201000271.
60. Mandal, D., Kim, K.J., and Lee, J.S. (2012). Simple synthesis of palladium nanoparticles, β-phase formation, and the control of chain and dipole orientations in palladium-doped poly(vinylidene fluoride) thin films. Langmuir *28*, 10310–10317. https://doi.org/10.1021/la300983x.
61. Cseri, T., Békássy, S., Kenessey, G., Liptay, G., and Figueras, F. (1996). Characterization of metal nitrates and clay supported metal nitrates by thermal analysis. Thermochim. Acta *288*, 137–154. https://doi.org/10.1016/S0040-6031(96)03037-7.
62. Richardson, H.W. (2000). Copper Compounds. In Ullmann's Encyclopedia of Industrial Chemistry (John Wiley & Sons, Ltd). https://doi.org/10.1002/14356007.a07_567. https://onlinelibrary.wiley.com/action/showCitFormats?doi=10.1002%2F14356007.a07_567&mobileUi=0.
63. Sumathirathne, L., and Euler, W.B. (2021). Catalysis of the Thermal Decomposition of Transition Metal Nitrate Hydrates by Poly(vinylidene difluoride). Polymers *13*, 3112. https://doi.org/10.3390/polym13183112.
64. Jaleh, B., Gavary, N., Fakhri, P., Muensit, N., and Taheri, S.M. (2015). Characteristics of PVDF membranes irradiated by electron beam. Membranes *5*, 1–10. https://doi.org/10.3390/membranes5010001.
65. de Jesus Silva, A.J., Contreras, M.M., Nascimento, C.R., and da Costa, M.F. (2020). Kinetics of thermal degradation and lifetime study of poly(vinylidene fluoride) (PVDF) subjected to bioethanol fuel accelerated aging. Heliyon *6*, e04573. https://doi.org/10.1016/j.heliyon.2020.e04573.
66. Rouquerol, J., Rouquerol, F., and Sing, K.S.W. (1998). Adsorption by Powders and Porous Solids: Principles, Methodology and Applications, 1 edition (Academic Press).
67. Webb, P.A., Orr, C., Camp, R.W., Olivier, J.P., and Yunes, Y.S. (1997). Analytical Methods in Fine Particle Technology, 1st edition (Micromeritics Instrument).
68. Plötze, M., and Niemz, P. (2011). Porosity and pore size distribution of different wood types as determined by mercury intrusion porosimetry. Eur. J. Wood Prod. *69*, 649–657. https://doi.org/10.1007/s00107-010-0504-0.
69. Wang, S., Yang, P., Dai, D., Xue, K., and Li, D. (2020). A study on micro-pore characteristics of clay due to freeze-thaw and compression by mercury intrusion porosimetry. Front.

Earth Sci. *7*, 344. https://doi.org/10.3389/feart.2019.00344.

70. Tõnurist, K. (2013). Influence of Electrospun Separator Materials Properties on Electrochemical Performance of Electrical Double-Layer Capacitors.
71. Tõnurist, K., Thomberg, T., Jänes, A., Kink, I., and Lust, E. (2012). Specific performance of electrical double layer capacitors based on different separator materials in room temperature ionic liquid. Electrochem. Commun. *22*, 77–80. https://doi.org/10.1016/j.elecom.2012.05.029.
72. Delumeau, L.-V., Asgarimoghaddam, H., Alkie, T., Jones, A.J.B., Lum, S., Mistry, K., Aucoin, M.G., DeWitte-Orr, S., and Musselman, K.P. (2021). Effectiveness of antiviral metal and metal oxide thin-film coatings against human coronavirus 229E. Apl. Mater. *9*, 111114. https://doi.org/10.1063/5.0056138.
73. Rihn, S.J., Merits, A., Bakshi, S., Turnbull, M.L., Wickenhagen, A., Alexander, A.J.T., Baillie, C., Brennan, B., Brown, F., Brunker, K., et al. (2021). A plasmid DNA-launched SARS-CoV-2 reverse genetics system and coronavirus toolkit for COVID-19 research. PLoS Biol. *19*, e3001091. https://doi.org/10.1371/journal.pbio.3001091.
74. Tõnurist, K., Thomberg, T., Jänes, A., Romann, T., Sammelselg, V., and Lust, E. (2013). Influence of separator properties on electrochemical performance of electrical double-layer capacitors. J. Electroanal. Chem. *689*, 8–20. https://doi.org/10.1016/j.jelechem.2012.11.024.
75. Tõnurist, K., Thomberg, T., Jänes, A., Romann, T., Sammelselg, V., and Lust, E. (2013). Polymorphic behavior and morphology of electrospun poly(vinylidene fluoride) separator materials for non-aqueous electrolyte based electric double layer capacitors. ECS Trans. *50*, 49–58. https://doi.org/10.1149/05045.0049ecst.
76. Balaram, V. (2020). Microwave plasma atomic emission spectrometry (MP-AES) and its applications – A critical review. Microchem. J. *159*, 105483. https://doi.org/10.1016/j.microc.2020.105483.
77. Hotaling, N.A., Bharti, K., Kriel, H., and Simon, C.G. (2015). DiameterJ: A validated open source nanofiber diameter measurement tool. Biomaterials *61*, 327–338. https://doi.org/10.1016/j.biomaterials.2015.05.015.
78. Holder, C.F., and Schaak, R.E. (2019). Tutorial on powder X-ray diffraction for characterizing nanoscale materials. ACS Nano *13*, 7359–7365. https://doi.org/10.1021/acsnano.9b05157.
79. Cai, X., Lei, T., Sun, D., and Lin, L. (2017). A critical analysis of the α, β and γ phases in poly(vinylidene fluoride) using FTIR. RSC Adv. *7*, 15382–15389. https://doi.org/10.1039/C7RA01267E.
80. Wu, T., Zhou, B., Zhu, T., Shi, J., Xu, Z., Hu, C., and Wang, J. (2015). Facile and low-cost approach towards a PVDF ultrafiltration membrane with enhanced hydrophilicity and antifouling performance via graphene oxide/water-bath coagulation. RSC Adv. *5*, 7880–7889. https://doi.org/10.1039/C4RA13476A.

STAR★METHODS

KEY RESOURCES TABLE

REAGENT or RESOURCE	SOURCE	IDENTIFIER
Bacterial and virus strains		
SARS-CoV-2 NG	Rihn et al.[73]	N/A
Chemicals,peptides, and recombinant proteins		
1% v/v Penicillin/Streptomycin stock solution	Gibco	#15070-063
Polyvinylidene difluoride	Sigma-Aldrich	427144; CAS: 24937-79-9
N,N-dimethylacetamide	Sigma-Aldrich	271012; CAS: 127-19-5
Copper(II) nitrate hemi(pentahydrate)	Sigma-Aldrich	467855; CAS: 19004-19-4
Experimental models: Cell lines		
VeroE6 (African green monkey epithelial kidney) cells	ATCC	RRID: CVCL_0574

RESOURCE AVAILABILITY

Lead contact

Further information and requests for resources and reagents should be directed to and will be fulfilled by the lead contact Thomas Thomberg (thomas.thomberg@ut.ee).

Materials availability

This study did not generate new unique reagents.

Data and code availability

- All data reported in this paper will be shared by the lead contact upon request.
- This paper does not report original code.
- Any additional information required to reanalyze the data reported in this paper is available from the lead contact upon request.

METHOD DETAILS

Spinning solution preparation

The polymer solution used in the experiments was prepared a day before the electrospinning. In order to dissolve the polymer faster, a magnetic stirrer with a heating plate (IKA C-MAG HS7) kept at 55°C was used. Polyvinylidene difluoride (PVDF, average molecular weight ~ 275 000 g mol^{-1}, Sigma-Aldrich) was used as a polymer, N,N-dimethylacetamide (DMA, anhydrous, purity 99.8%, Sigma-Aldrich) as a solvent, and copper salt ($Cu(NO_3)_2 \cdot 2.5H_2O$, purity ≥ 99.99%, Sigma-Aldrich) was added to the solution as a virucidal component. The concentration of the polymer in the solution was 28 weight percentage (wt%), and the wt% of the salt varied from 0.25 wt%, 0.75 wt%, 2.0 wt% to 3.5 wt%, respectively.[27–30,45,74,75]

Electrospun filter materials preparation

The electrospinning method was used to produce virucidal filter materials. The apparatus of the electrospinning method consisted of a high voltage source, a syringe pump, a syringe (10 ml), a syringe needle (with an inner diameter of 0.4 mm), a system for moving the needle horizontally, a cylindrical rotating collector (diameter 9 cm), and a climate control unit controlling the temperature and humidity (EC-DIG, IME Technologies, Netherlands). In all experiments, the temperature was set at 23 ± 1°C, humidity 60 ± 3%, solution feed rate 1 ml h^{-1}, needle movement speed 5 cm s^{-1} with a delay of 0.5 s at the ends, collector rotation speed 500 rpm and the distance of the needle from the collector was 9 cm. The voltage applied to the solution was gradually increased by 2 kV increments from 11 to 21 kV in order to find suitable electrospinning conditions for the production of metal nanocluster containing nanofibrous materials (Table 1). For electrospinning the metal nanocluster free filter material, the voltage was kept at 9 kV because at higher voltages it was impossible to get a mat with nanofibrous structure.[45] The collector was covered with aluminum foil to collect the filter materials, and different volumes of solution were used for their preparation.[27–30,45,74,75]

Physical characterization of electrospun filter materials

The filter materials' structure, morphology, elemental composition, and element distribution were studied with a scanning electron microscope (SEM) Zeiss EVO MA15 system with an Oxford X-MAX 80 energy dispersive detector (EDS). Before SEM and EDS analyses, the surface

of the filter materials was covered with either a few nanometers of thick platinum or carbon layers, respectively. The content of copper in the filter materials was analyzed by the MP-AES method using the Agilent 4210 system.[76] For analysis, the sample was weighed into a 25 cm^3 PFA (perfluoroalkoxy alkane) sealed container, adding 10 cm^3 of 69% HNO_3 (Carl Roth Rotipuran Supra), and heated for 24 h at 105°C. After dissolution, the samples were diluted with 2 wt% HNO_3 solution to the expected Cu content of 4 mg dm^{-3}. Quantification was performed at a wavelength of Cu 327.395 nm in three replicates, and the signal was collected for 10 s in each replicate. A calibration chart was used in the range of 0.1-10 mg dm^{-3}, and calibration solutions with a concentration of 1 g dm^{-3} were prepared from an Agilent multi-element calibration standard 2A solution. The fiber diameters were determined based on SEM images using the free software ImageJ, and the fiber size distribution was compiled using the diameters of 40 fibers from each filter material.[77]

Nitrogen sorption analysis was used to characterize the porous structure of filter materials, which was performed at the boiling temperature of liquid nitrogen (-195.8°C) with the ASAP 2020 system (Micromeritics, USA). Based on the Brunauer-Emmett-Teller (BET) theory, the specific surface areas (S_{BET}) of the filter materials were calculated in the range of relative pressures (p/p_0) between 0.05–0.1. The filter materials' total pore volume (V_{sum}) was calculated according to the amount of nitrogen adsorbed on the sample at a relative pressure of p/p_0 = 0.95.[57,66]

The mercury intrusion porosimetry method was also used to characterize the porous structure of the filter materials. The measurements were performed with an AutoPore IV instrument (Micromeritics, USA), and triple distilled mercury with a purity of 99.9995% was used.[67–69] The volume of the sample holder was 3 cm^3, and the stem volume was 0.412 cm^3. The samples were degassed under vacuum at 100°C for at least one hour before measurements. Mercury porosimetry curves were measured within the pressure range from 0.01 to 410 Mpa by recording the amount of mercury intruded into the sample at each measured pressure. The blank sample data was subtracted from the measurement results, taking into account the effect of temperature and the sample holder from the analysis results, and the average results were found from repeated measurements of the filter materials.

Thermogravimetric analysis (TGA) was used to analyze the thermal stability of the filter materials by using a NETZSCH STA 449 F3 instrument and an Al_2O_3 sample holder. The parameters of the TGA experiment were as follows: temperature range 25°C – 1000°C, heating rate 10°C min^{-1}, and gas flow rate 50 cm^3 min^{-1}. The stability of the materials was determined both in an inert gas (nitrogen, 99.999%, Linde Gas) and synthetic air containing 20% oxygen by volume (99.999%, Linde Gas).[45]

X-ray diffraction analysis (XRD) was used to analyze the crystalline structure of the filter materials, and measurements were performed on a Bruker D8 instrument (Bruker Corporation) at a temperature of 25 ± 1°C. A CuKα radiation source was used with a LynxEye position sensitive detector, where the angular step was 0.01° and the counting time for each angle was 2 s.[78–80]

The hydrophobicity of the filter materials was established by pipetting a droplet of ultrapure water (Milli-Q+, resistivity 18.2 MΩ cm) onto the surface of the filter material and by measuring the contact angle between the filter material surface and a water droplet.[70]

Electrospun filter materials particle filtration efficiency and breathability

In order to analyze the filter materials' filtration efficiency, experiments were carried out on a self-designed system. A detailed description of the particle filtration efficiency (PFE) tests and apparatus scheme can be found elsewhere.[27,45] Briefly, the aerosol for calibration was generated with an atomizer from the dispersion of polystyrene latex spheres with a diameter of 3 μm (Thermo Scientific, Lot No. 212695(net) 3 μm) in distilled water. Aerosol flow was measured before and after sample measurements, and silica gel was used to dry it. Two different instruments were used to measure the entire aerosol particle size range: for the size range of 5–500 nm, FMPS (Fast mobility Particle Spectrometer, TSI Incorporated) was used, and for 300 nm – 10 μm size range OPS (Optical particle counter, TSI incorporated) system was employed. A gas flow rate meter (4140, TSI) was used to measure the air flow rate, and it was controlled by a two-way Bürkert 2/2 solenoid valve (no. 00234303, Christian Bürkert GmbH). The air flow rate in the conducted experiments was 1.8 dm^3 min^{-1} per 4.9 cm^2 filtration area, and the concentration of aerosol particles (particles per liter) was determined before B_b and after the measurement B_a of each sample, from which the average concentration value was found. Filter materials were measured in three parallel experiments, and the average filtration efficiency was calculated. The filtration efficiency (E, unit %) was calculated based on the following equation:

$$E = 100\% \frac{\left(\frac{B_b + B_a}{2}\right) - T}{\left(\frac{B_b + B_a}{2}\right)}$$

where T is the concentration of aerosol particles passing through the filter.

The breathability of the filter material was evaluated using the pressure drop value, which was measured according to the EN 14683:2019+AC:2019 standard. Unlike the 14683:2019+AC:2019 standard, measurements were not performed at a relative humidity of 85%. The sample (filter material) was placed between the metal filter holder, and the pressure difference caused by the material was measured. The breathability tests were conducted in triplicate. Three different areas were chosen to be tested from all the electrospun samples.

Virus strain and virucidal activity determination

In order to study the virucidal properties of the filter materials, a recombinant SARS-CoV-2 (Wuhan-Hu-1 strain), in which the gene encoding the spike protein was replaced by that of the alpha variant, was used. To facilitate the visualization of infected cells, a mNeonGreen marker was

attached to the C terminus of the ORF7a protein of the virus, hereafter designated as SARS-CoV-2 NG[73]. The virus was propagated in VeroE6 (African green monkey epithelial kidney) cells grown in Dulbecco's Modified Eagle's Medium (DMEM, Corning, #10-013-CV) supplemented with 0.2% w/v BSA (bovine serum albumin, Sigma-Aldrich) and 1% v/v Penicillin/Streptomycin stock solution (Gibco, #15070-063), hereafter virus growth medium (VGM). The virus titer was determined on the same cells using the $TCID_{50}$ (median tissue culture infectious dose 50) test and was calculated using the Spearman-Karber algorithm.

Determination of the virucidal properties of the electrospun filter materials was performed according to the ISO 21702:2019 standard with modifications. Virucidal properties were determined for PVDF filter materials with 0.25 wt%, 0.75 wt%, 2.0 wt%, or 3.5 wt% $Cu(NO_3)_2 \cdot 2.5H_2O$ added to the spinning solution. A reference material without salt addition (unmodified PVDF filter material) was used as a control sample. Before the experiments, all samples were treated with UV-C radiation to clean them from possible contamination. The stock solution of SARS-CoV-2 NG (concentration $\sim 7 \times 10^7$ $TCID_{50}$ units ml^{-1}) was diluted 10 times in phosphate buffered saline (PBS). The 30 mm x 30 mm electrospun filter material and reference material pieces were inoculated with 200 μl of the virus suspension and covered with a piece of PVC (poly(vinyl chloride), dimensions 20 mm x 20 mm) to ensure even distribution of the suspension. The samples were incubated for 0, 1, 2, 4, 8, or 12 hours at 25 $\pm$ 2°C, and after that, the samples were washed with 10 ml of VGM solution. The concentration of infectious virus in each wash-out was determined using the $TCID_{50}$ assay. All samples' average titer values were calculated based on at least three independent experiments. The decrease in virus concentration $\Delta \log c$ was calculated according to the following equation: $\Delta \log c = \log(c_{0h}) - \log(c_{xh})$, where c_{0h} and c_{xh} are virus concentrations at the contact time of 0 h and *x* h, respectively, and *x* in our experiments was either 1, 2, 4, 8, or 12 hours.

The stability of the electrospun filter materials was evaluated based on the maintenance of their virucidal activity. For these experiments, the electrospun filter material prepared using 28 wt% PVDF + DMA + 2.0 wt% $Cu(NO_3)_2 \cdot 2.5H_2O$ spinning solution; a contact time of 8 h was selected for virucidal assay due to the substantial virucidal effect observed in previous assays. The virucidal activity of the selected material under these conditions was evaluated immediately after the preparation of the material and then 1, 2, and 3 months after the first tests. All materials tested were pre-cut into size (30 mm x 30 mm), followed by double-sided UV-C treatment to reduce contamination, and stored at room temperature in a dry, dark place until further testing.